The Astrophysical Journal Letters, 709:L142–L145, 2010 February 1 doi:10.1088/2041-8205/709/2/L142

DUAL-STAGE RECONNECTION DURING SOLAR FLARES OBSERVED IN HARD X-RAY

Yan Xu[1], Ju Jing[1], Wenda Cao[2], and Haimin Wang[1]
[1] Space Weather Research Lab, Center for Solar-Terrestial Research, New Jersey Institute of Technology, 323 Martin Luther King Blvd, Newark, NJ 07102-1982, USA; yx2@njit.edu
[2] Big Bear Solar Observatory, 40386 North Shore Lane, Big Bear City, CA 92314, USA
Received 2009 August 17; accepted 2009 December 28; published 2010 January 12

ABSTRACT

In this Letter, we present hard X-ray (HXR) observation by the *Reuven Ramaty High Energy Solar Spectroscopic Imager* of the 2003 October 29 X10 flare. Two pairs of HXR conjugate footpoints have been identified during the early impulsive phase. This geometric configuration is very much in the manner predicted by the "tether-cutting" scenario first proposed by Moore & Roumeliotis. The HXR light curves show that the outer pair of footpoints disappeared much faster than the other pair. This temporal behavior further confirms that this event is a good example of the "tether-cutting" model. In addition, we reconstructed a three-dimensional magnetic field based on the nonlinear force-free extrapolation and found that each pair of HXR footpoints were indeed linked by corresponding magnetic field lines.

Key words: Sun: activity – Sun: flares – Sun: X-rays, gamma rays

1. INTRODUCTION

Motions in and around a solar flare imply restructuring of the plasma needed to release energy from the magnetic field. In large-scale reconnection models, the plasma adjusts itself so that magnetic flux suddenly moves from one domain of connectivity to another. This is the process termed magnetic reconnection in the theory of magnetized plasmas. Although the physics of reconnection has to be understood at the microscopic level, in which one can fully understand the behavior of the waves and particles involved, the consequences are macroscopic. Thus simplifying ideas have emerged, such as "loop–loop interaction," "emerging flux," "patchy reconnection," and "breakout" (see the Cartoon Archive at http://solarmuri.ssl.berkeley.edu/hhudson/cartoons/). Note that there are other schemes not represented in the Cartoon Archive, especially the "tether-cutting" reconnection. Each model prescribes characteristic patterns of large-scale plasma motions, which are best interpreted in terms of the three-dimensional structure of the coronal magnetic fields.

In this study, we describe a flare that develops very much in the manner as predicted by the "tether-cutting" scenario long championed by Moore & Roumeliotis (1992). A modified configuration with bipoles having sigmoidally sheared and twisted core fields was shown by Moore et al. (2001). In this picture short, low-lying fields reconnect bit by bit, each time adding to a magnetic flux tube (or flux rope, since it carries a field-aligned current that Ampere's Law identifies with a twist in the magnetic field). Eventually these "tethers"—originally helping to hold down the flux–rope structure—become so weak that they erupt. As observational evidence, eruptive filaments and sigmoid structures are always analyzed in studies relevant to the "tether-cutting" model. Most observations of sigmoid structures associated with eruptive events were obtained in Hα, soft X-ray (SXR), and EUV wavelengths (Liu et al. 2007b; Sterling & Moore 2004, 2005; Sterling et al. 2007; Kim et al. 2008; Yurchyshyn et al. 2006). Hard X-ray (HXR) loop-top sources have also been compared with prominence eruptions close to solar limb by Chifor et al. (2006, 2007) and Liu et al. (2009b). Their results show that HXR sources were located below the apex of the associated prominence, which is consistent with the scenario of the "tether-cutting" model. However, signatures of multiple flare footpoints, especially two far-end footpoints for events close to the disk center, which is also an important implication predicted by the "tether-cutting" model, have never been identified from previous observations. The disk event studied in this Letter has four HXR feet in the lower atmosphere. It was observed in several wavelengths. Particularly, the flare emission from visible and near-infrared (NIR) continua, along with HXR in high-energy bands up to 300 keV (Xu et al. 2006), shows strong evidence of precipitation of a nonthermal electron along the reconnected loops. The motions of two major footpoints have been analyzed by Liu et al. (2009a) and Des Jardins et al. (2009). A sigmoid structure was also identified and studied by Ji et al. (2008). Our goal is to analyze the HXR footpoints and their temporal evolution showing two distinct stages of reconnection, which could be explained by the "tether-cutting" model.

2. OBSERVATION AND DATA REDUCTION

The flare we study in this Letter, categorized as *GOES* X10 class on 2003 October 29, was one of the most powerful events of solar cycle 23. The spatially integrated intensity reached the first impulsive peak around 20:42 UT. Therefore, most ground-based telescopes in the U.S. and Europe, as well as the space telescopes, had a good coverage of it. Its emission covers a wide range of the entire electromagnetic spectrum, from radio to gamma rays. Particularly, it is the first flare detected in the NIR continuum (Xu et al. 2004). Their Figure 2 shows highly correlated HXR and NIR emission (both spatially and temporally) during the impulsive phase. This figure along with their Figure 3 gives a basic idea of flare ribbon development and separation in both NIR and HXR.

Normally, the *Reuven Ramaty High Energy Solar Spectroscopic Imager* (*RHESSI*; Lin et al. 2002) provides spatial information by synthesizing the time-modulated signals from a set of nine rotating modulation collimators (RMCs; Hurford et al. 2002). In our case, all the nine RMCs are included for the image reconstruction using the CLEAN algorithm. This combination of RMCs yields the finest resolution of about 5.″9 (Liu et al. 2007a). Due to the high-spatial-resolution setup of NIR

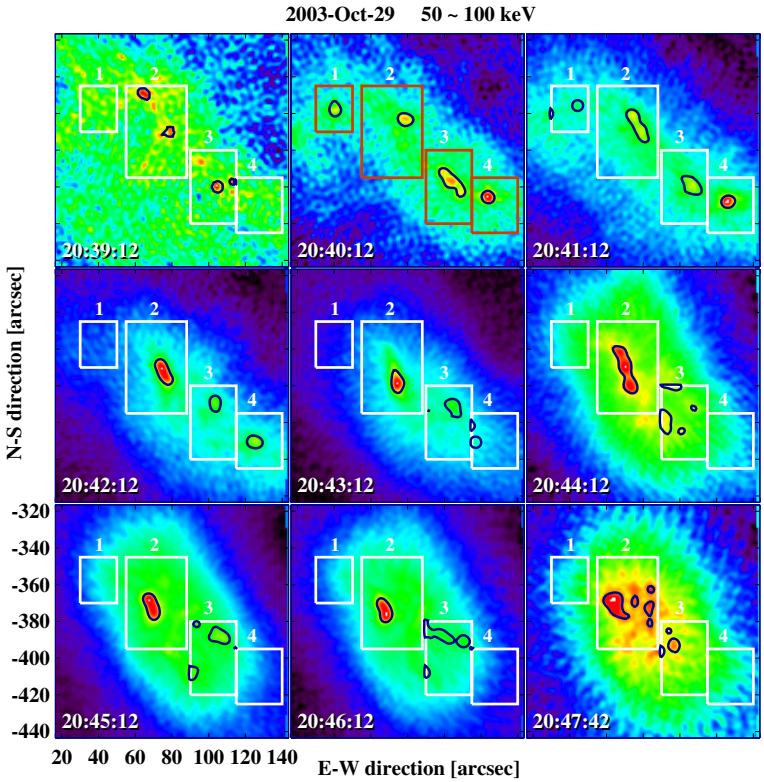

Figure 1. *RHESSI* HXR CLEAN images obtained on 2003 October 29 from 20:39:12 to 20:47:42 UT. The integration time is 30 s and the photon energy range is 50–100 keV. Four HXR sources are identified and marked with boxes 1–4. Red boxes at 20:40 UT emphasize weak sources 1 and 4 at their peak time. Black contours indicate CLEAN component within each box.

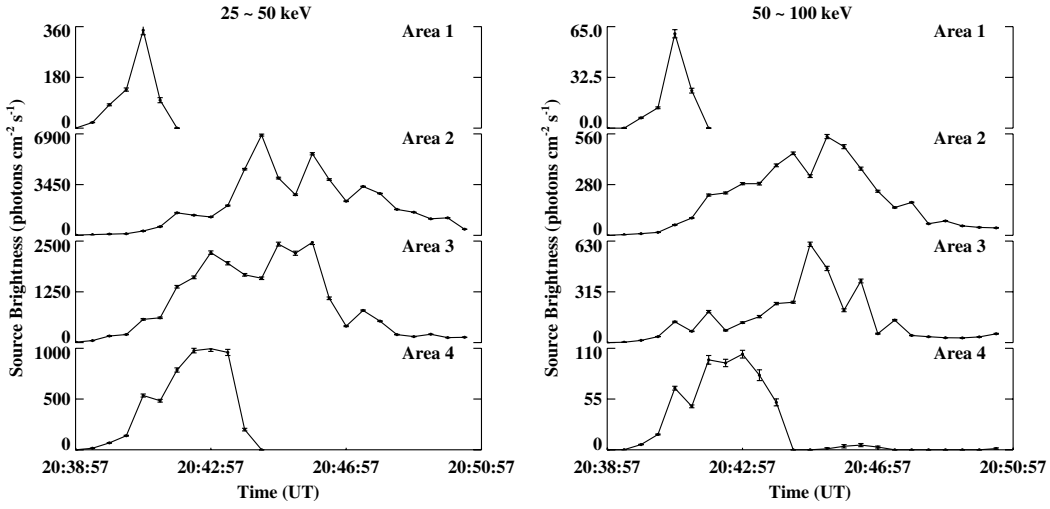

Figure 2. Light curves of HXR sources 1–4 with energy ranges of 25–50 keV (left) and 50–100 keV (right).

observation, the field of view (FOV) was restricted to $91'' \times 91''$ in Xu et al. (2004, 2006). For comparison, HXR images were generated within the same FOV covering three HXR sources in previous studies. In addition, an enlarged FOV of $128'' \times 128''$ was generated in this study, in which one more HXR source becomes evident. Figure 1 shows HXR CLEAN images with an energy band of 50–100 keV and integration time intervals of 30 s. It is clear that four HXR footpoint kernels, within red boxes in Figure 1, appeared around 20:40:42 UT. Four corresponding areas of all HXR sources are marked with white boxes 1–4 at other time intervals, i.e., none of the HXR kernels moved out of their boxes during the entire period. We use CLEAN component maps to locate HXR sources within the boxes at each time interval, as suggested by Dennis & Pernak (2009). The outer pair (1 and 4) of footpoints was relatively weaker and decayed very quickly. Conversely, the inner two (2 and 3) were much stronger and decayed slowly. Previous studies (Xu et al. 2004, 2006; Liu et al. 2009a; Des Jardins et al. 2009) concentrated on these strong kernels. Nonetheless, Xu et al. (2004) found the corresponding NIR emission of HXR source 4, and Des Jardins et al. (2009) confirms that source 4 is independent of source 3. It also disappeared earlier than sources 2 and 3 in white light. HXR light curves (spatially integration of CLEAN maps) of each area are plotted in Figure 2 with energy bands of 25–50 keV

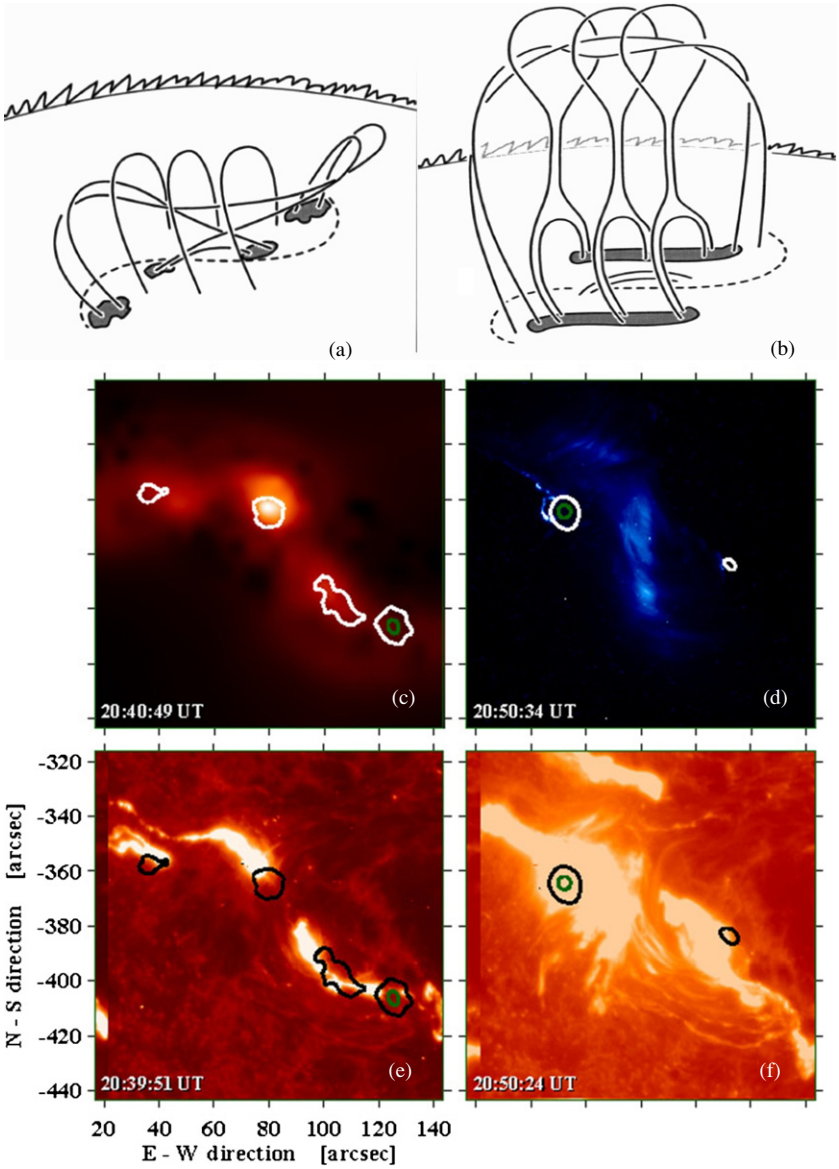

Figure 3. Top panels (a) and (b): beginning and midlife stages of an eruptive magnetic configuration of "tether-cutting" model (adopted with authorization from Moore et al. 2001). Mid panels (c) and (d): HXR contours (white: 45%, green: 85%) over the backgrounds of SXI SXR image (left) and *TRACE* EUV 195 Å image (right) at 20:40:49 UT and 20:50:34 UT, respectively. Bottom panels (e) and (f): HXR contours (white: 45%, green: 85%) over the backgrounds of *TRACE* 1600 Å image at 20:39:51 UT (left) and 20:50:24 UT (right).

(left) and 50–100 keV (right). As shown in Figure 2, kernels 1 and 4 peaked/disappeared earlier than the other pair (kernels 2 and 3), which indeed provides strong support for the prediction of the "tether-cutting" model. The uncertainty σ of each individual pixel is calculated using $\frac{1}{6}$ of the maximum emission in the FOV excluding the source regions (Saint-Hilaire et al. 2008). Hence, the overall uncertainty of an entire source is $\sqrt{N} \times \sigma$, where N is the number of pixels of a certain HXR source. More sophisticated algorithms of error estimation could be found in Liu (2008).

Upper panels of Figure 3, which are adopted from Moore et al. (2001), illustrate the temporal magnetic evolution of two reconnection stages. At the beginning, accelerated particles penetrate down along two sets of reconnected field lines and produce emission from four footpoints; see panel (a). Panel (b) shows the second step of a well-developed erupting system with reconnection of less sheared field lines. Therefore, two flare ribbons become conspicuous other than several single footpoints. These two sketches match well with the observed configuration shown in the lower panels of Figure 3. Panel (c) shows the first stage of four separated sources in HXR. The contours are 45% (white) and 85% (green) to the maximum HXR emission and the background is an SXR image from the *GOES* Solar X-ray Imager (SXI) taken at 20:40:49 UT. All HXR sources locate along the SXR sigmoid structure, which has been reported by Ji et al. (2008). The *Transition Region and Coronal Explorer* (*TRACE*) EUV 195 image in panel (d) shows the well-developed flare loops above the magnetic neutral line separating the HXR conjugate footpoints. In white-light observation, they appear to be elongated ribbons other than compact footpoints. Due to the dynamic range problem, most flare ribbons are imaged as kernels in HXR by *RHESSI*, except a few specific events (see Liu et al. 2007a). Panels (e) and (f) show two *TRACE* 1600 Å images in the background. The black contours are again from HXR 45% (black) and 85% (green) to the maximum. The *TRACE* images

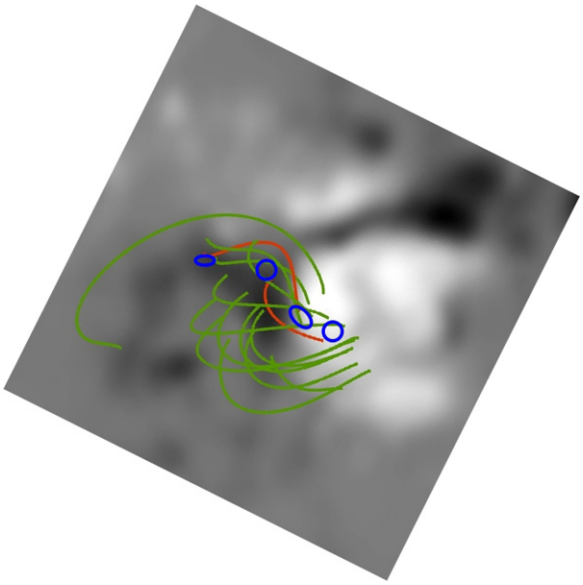

Figure 4. NLFF extrapolation of an MSFC's vector magnetogram (background) taken at 18:31 UT. It has been rotated by ∼25° to compensate for solar *P*-angle. Reconstructed magnetic field lines are plotted in green and red colors. The latter field lines indicate the connections between HXR sources (blue).

confirm the existence of four individual footpoints, especially source 1 is separated from source 2 at the beginning of the flare.

In addition to the two-dimensional observations, we extrapolated the three-dimensional nonlinear force free (NLFF) magnetic field by applying the weighted "optimization" method (Wiegelmann 2004) to NASA Marshall Space Flight Center's (MSFC's) vector magnetograms. As shown in Figure 4, the FOV here is 284″ × 284″ with a pixel resolution of 1.″29 (or ∼940 Km) in all three dimensions. To avoid the "magnetic transient" problem (Patterson & Zirin 1981) of magnetograms during solar flares, we chose the vector magnetogram taken at 18:31:42 UT and differential-rotated it to the flare time at 20:40:49 UT. The extrapolated magnetogram was rotated by about 25° to compensate for solar *P*-angle and aligned to a full disk MDI magnetogram by matching magnetic structures. Therefore, we can locate HXR footpoints (blue) on the vector magnetogram and the extrapolated field lines. It is clear that footpoints 1 and 3 are connected (see red field lines) and 2 and 4 are the other conjugate pair. Again, a similar geometric configuration before the "onset" eruption could be found in Figure 3.

3. DISCUSSION

We present the very first observation of four footpoint sources and their temporal evolution in HXR. All of HXR footpoints co-exist within a short period of 1 or 2 minutes. Note that the multiple HXR kernels do not belong to two ribbons, like the case presented by Liu et al. (2007a). The reasons are: first, source 1 locates more than 40″ away from source 2, which is too far for a single HXR ribbon. Also, in *TRACE* 1600 Å image, HXR sources 1 and 2 have distinct counterparts. So, sources 1 and 2 are different footpoints. Second, as shown in Figure 3 in Xu et al. (2004), sources 3 and 4 located in the same magnetic polarity, but moving oppositely (one was moving toward the magnetic neutral line and the other was moving away from the neutral line). Therefore, we believe that there are four HXR footpoints which are connected pairwise. This is just the arrangement anticipated for magnetic flux tubes reconnecting in a tether-cutting scenario, which should result in four discrete HXR footpoints. The model also predicts the evolution of footpoints. As the flare develops, two flare ribbons will be formed instead of four footpoints. This is also observed and shown in Figure 3.

In several models of solar flares, the large-scale deformation of the magnetic field is assumed to involve magnetic reconnection in a direct way. "Tether-cutting" has long been one of the favored scenarios. We have found this scenario to fit this strong and well-studied flare. The main significance of this observation is that it reveals the complex geometric configuration and evolution during the early phase of an impulsive flare. It also ties the "tether-cutting" scenario to the HXR footpoint sources observed by *RHESSI*, which guide us to the main energy release of a flare.

The authors sincerely thank the anonymous referee for his/her suggestions to improve this Letter. The authors thank Drs. Hugh Hudson and Ron Moore for valuable discussion and Dr. Wei Liu for suggestion regarding *RHESSI* imaging and error estimation. This work is supported by NASA under grants NNX08-AJ23G and NNX07-AH78G. J.J. was supported by NSF under grant ATM 09-36665 and ATM 07-16950. W.C. gratefully acknowledges the support of NSF through ATM-0847126.

REFERENCES

Chifor, C., Mason, H. E., Tripathi, D., Isobe, H., & Asai, A. 2006, A&A, 458, 965
Chifor, C., Tripathi, D., Mason, H. E., & Dennis, B. R. 2007, A&A, 472, 967
Dennis, B. R., & Pernak, R. L. 2009, ApJ, 698, 2131
Des Jardins, A., Canfield, R., Longcope, D., Fordyce, C., & Waitukaitis, S. 2009, ApJ, 693, 1628
Hurford, G. J., et al. 2002, Sol. Phys., 210, 61
Ji, H., Wang, H., Liu, C., & Dennis, B. R. 2008, ApJ, 680, 734
Kim, S., Moon, Y.-J., Kim, Y.-H., Park, Y.-D., Kim, K.-S., Choe, G. S., & Kim, K.-H. 2008, ApJ, 683, 510
Lin, R. P., et al. 2002, Sol. Phys., 210, 3
Liu, C., Lee, J., Gary, D. E., & Wang, H. 2007a, ApJ, 658, L127
Liu, C., Lee, J., Yurchyshyn, V., Deng, N., Cho, K.-s., Karlický, M., & Wang, H. 2007b, ApJ, 669, 1372
Liu, W. 2008, Solar Flares as Natural Particle Accelerators: A High-energy View from X-ray Observations and Theoretical Models (Saarbrücken: VDM Verlag)
Liu, W., Petrosian, V., Dennis, B. R., & Holman, G. D. 2009a, ApJ, 693, 847
Liu, W., Wang, T.-J., Dennis, B. R., & Holman, G. D. 2009b, ApJ, 698, 632
Moore, R. L., & Roumeliotis, G. 1992, in IAU Coll. 133, Eruptive Solar Flares, Lecture Notes in Physics 399, ed. Z. Svetska, B. V. Jackson, & M. E. Machado (New York: Springer), 69
Moore, R. L., Sterling, A. C., Hudson, H. S., & Lemen, J. R. 2001, ApJ, 552, 833
Patterson, A., & Zirin, H. 1981, ApJ, 243, L99
Saint-Hilaire, P., Krucker, S., & Lin, R. P. 2008, Sol. Phys., 250, 53
Sterling, A. C., & Moore, R. L. 2004, ApJ, 613, 1221
Sterling, A. C., & Moore, R. L. 2005, ApJ, 630, 1148
Sterling, A. C., et al. 2007, PASJ, 59, 823
Wiegelmann, T. 2004, Sol. Phys., 219, 87
Xu, Y., Cao, W., Liu, C., Yang, G., Jing, J., Denker, C., Emslie, A. G., & Wang, H. 2006, ApJ, 641, 1210
Xu, Y., Cao, W., Liu, C., Yang, G., Qiu, J., Jing, J., Denker, C., & Wang, H. 2004, ApJ, 607, L131
Yurchyshyn, V., Karlický, M., Hu, Q., & Wang, H. 2006, Sol. Phys., 235, 147